Journal of
Synchrotron Radiation

ISSN 0909-0495

Received 2 December 2006
Accepted 12 June 2007

Combining two structural techniques on the micrometer scale: micro-XAS and micro-Raman spectroscopy

V. Briois,[a] D. Vantelon,[a] F. Villain,[a,b] B. Couzinet,[c] A.-M. Flank[a] and P. Lagarde[a]*

[a]Synchrotron SOLEIL, BP 48, 91192 Gif sur Yvette, France, [b]CIM2, Université Pierre et Marie Curie Paris VI, 4 Place Jussieu, 75252 Paris CEDEX 05, France, and [c]PMD, IMPMC, Université Pierre et Marie Curie Paris VI, 140 Rue de Lourmel, 75015 Paris, France.
E-mail: pierre.lagarde@synchrotron-soleil.fr

X-ray absorption and Raman spectroscopies are complementary in the sense that both give very precise information about the local structure of a sample, both are not restricted to crystalline materials, and in both cases the volumes of the material probed are similar. The X-ray technique has the advantage of being element- and orbital-selective, and sensitive to orientational effects owing to polarization selection rules. In many cases, however, its analysis can present some ambiguity. Combining the two techniques on a micrometer scale could therefore be a very powerful method structurally. In this paper the experimental set-up developed at the LUCIA beamline and its application to a natural mineral are described.

Keywords: X-ray absorption spectroscopy; Raman spectroscopy; microspectroscopy.

1. Introduction

During the last few years, experiments devoted to micro-analysis have been developed at many third-generation synchrotron radiation facilities by taking advantage of the increasing spectral brightness of the photon source. These new techniques, which are a natural evolution of the well established X-ray absorption spectroscopy (XAS), X-ray fluorescence (XRF) and X-ray diffraction (XRD) techniques, are aimed to give a much more detailed insight into heterogeneous materials. They are currently applied to samples (natural samples, micro-structured artefacts) for which the relevant scale is typically the micrometer. As these samples become more complex, analysis by a local structural method like XAS becomes more and more ambiguous since, even on this scale, the sample either could be made of several different crystallographic phases or the structural disorder could blur the full signature of the local environment. This level of complexity is increased further when the evolution of such a system under the influence of external parameters is of interest and when there are reasons to believe that the response of the whole system is due to well defined regions of the sample.

Therefore, in order to remove possible ambiguities of XAS analysis, it appears of fundamental importance to strengthen the conclusions arising from this structural technique with others from independent measurements obtained simultaneously at the same location. The results from one technique can be used as external constraints on the analysis of data from another technique. These new requirements of materials science studies are at the origin of the development of coupled micro-X-ray absorption (μ-XAS) and micro-Raman (μ-Raman) experiments that we have undertaken on the LUCIA beamline at the Swiss Light Source. These techniques have already been combined on a macro scale (a few tenths of a millimeter) (Briois, Belin *et al.*, 2005; Briois, Lützenkirchen-Hechta *et al.*, 2005, and references therein) and at this time the main purpose was to follow, with a precise time scale for instance, the evolution of a sample under external conditions. Time and/or temperature changes of the sample were then followed simultaneously with XAS, Raman and UV–visible spectroscopies and differential scanning calorimetry. Here we aim to add the spatial parameter to these experiments. During the last few years, a similar motivation has seen the combination of micro-diffraction (μ-XRD) with μ-XAS, as well as μ-XRD with μ-Raman spectroscopy (Davies *et al.*, 2005) and micro X-ray absorption with microtomography (Schroer *et al.*, 2005).

Raman spectroscopy is a well established technique which provides information on the local symmetry and the local atomic structure. Being sensitive to local bonds as well as to molecular units, its results appear complementary to those extracted from an EXAFS experiment, which is one of the best techniques for providing the description of the local environment of one given element. As is the case for X-ray diffraction, the Raman spectra of many organic or inorganic compounds have been gathered in several databases, and this can provide strong guidelines for XAS analysis. Similarly,

XAS analysis is grounded on the study of model compounds which have a well defined signature. The key point here is to have information at the same time from exactly the same location in the sample, this area being as small as possible for a precise description of the system.

2. Experimental set-up

The X-ray beam was delivered by the LUCIA beamline (Flank *et al.*, 2006). By using a double-crystal Si(111) monochromator, we could set the beam to a size of about 7 μm × 5 μm (horizontal × vertical), using two mirrors in a Kirkpatrick–Baez (KB) configuration, in order to match the expected size of the Raman exciting laser beam. The X-ray absorption signal was monitored by the X-ray fluorescence detected in the horizontal plane by a silicon drift diode. The resolution of this diode amounts to 100 eV at the silicon fluorescence. The different fluorescence lines are discriminated using a multichannel analyzer and their intensity directly obtained from the area of the XRF spectra. The X-ray experiments (cartography or spectroscopy) used a dwell time of typically 1 s.

Raman data have been collected using a RXN1-785 Raman spectrometer from Kaiser Optical Systems Inc. (KOSI) equipped with a near-IR laser diode working at 785 nm as excitation light, and with a CCD detector for providing a fast and simultaneous full spectral collection of Raman data from 100 to 3450 cm^{-1}. The collection of Raman data is ensured using the patented HoloPlex transmission grating from KOSI, which provides a typical spectral resolution of 2 cm^{-1}. The excitation by the laser is provided through a single-mode optical fiber whereas the collection of the Raman signal measured in back-scattering geometry is ensured through a multi-mode fiber, both being connected to a laser probehead equipped with holographic Notch filters. Note that the use of optical fibers, without additional inclusion of polarization optics in the probehead to create plane-polarized excitation light, leads to the recording of unpolarized Raman spectra. The power of the laser beam at the sample position was measured in a separate experiment to be 10 mW. To achieve a 5 μm laser spot size at the sample position, a 50× Olympus long-working-distance objective (numerical aperture 0.45) was used to focus the incident beam on the sample located at about 15 mm. Typical collection times for a Raman spectrum are of a few seconds, and co-additions of a few spectra are sometimes required to improve the signal-to-noise (S/N) ratio. In the case of the minerals studied herein, the collection time was 50 s (ten spectra, each integrated over 5 s) whereas a good S/N ratio can be achieved for pure silicon in 5 s.

Several geometrical constraints were taken into account when aligning both micrometer beams at the same sample point. Given the low energy of the X-rays, the whole XAS experiment is under vacuum with a flange equipped with a thin beryllium window isolating the ultra-high vacuum in the KB chamber from the conventional vacuum of the experimental part (10^{-2} torr). The small distance between this flange and the X-ray spot position (about 9 cm) limits the available space in front of the sample for the objective lens used for focusing the laser beam at the same incidence as the X-rays. We then had to use an incidence angle on the sample of 45° for the two beams, with the laser beam being vertical, at the expense of the ultimate size of the two spots. Owing to the convergence of the laser at the exit of the Raman probehead, the objective lens had to be located inside the vacuum chamber at the end of a 30 cm-long inox tube, itself connected to the probehead.

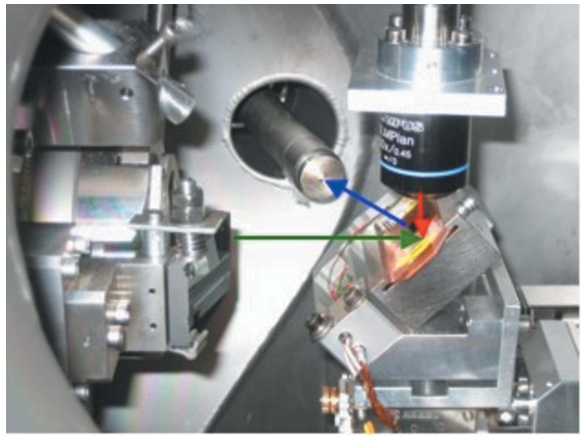

Figure 1
The μ-XAS Raman experiment set-up. The whole assembly, except the Raman spectrometer, is in the vacuum of the experimental chamber. Arrows: green = X-ray input beam, red = laser beam, blue = X-ray fluorescence.

Since the focused spot of the X-ray beam is kept fixed at one given position determined by the KB optics, the optical adjustment had to be made through an adjustment of the laser beam, by means of an (X', Y', Z') manipulator which sets the position of the objective lens connected to the optical Raman probehead. The sample itself could also be adjusted with regard to the two photon beams. A photograph of the assembly is given in Fig. 1.

3. Beam confocality

The confocality test was carried out on a set of 20 nm-thick titanium dots of various sizes with diameters ranging from 100 to 2 μm, deposited onto a pure silicon wafer (Thompson *et al.*, 2001). Raman spectroscopy of silicon gives a very strong and very well characterized signal at 521 cm^{-1} which comes, with the used objective lens and laser wavelength, from a shallow depth below the sample surface, of the order of 2 μm in the best cases. We can then consider, because of the accuracy of the vertical manipulator which sets the altitude of the probehead, that the cross section of the laser spot amounts to about 5 μm at the sample position. The Raman signature of silicon is therefore a good test of the correct focusing of the Raman optics, and this tuning is obtained by a vertical adjustment of the Raman optics head. On the another hand, the size of the X-ray beam, as a preliminary, has been measured at the sample position using the knife-edge technique and its value is set to about 7 μm (horizontally) and 5 μm (vertically). By setting the beamline energy just above the titanium *K*-edge, at around 5 keV, the dots allow the

measurement of the X-ray beam position and control of the size through a simultaneous recording of the Ti and Si fluorescence signals. Therefore the alignment of the whole assembly had to be carried out in two steps. The sample holder can be moved by stepping motors along the X-ray beam (Y), along the vertical (Z) and along the normal (X) to the (YZ) plane. At first the two beams are shone on a YAG crystal where both the X-ray and the laser beam could be optically detected by the beamline microscope. This position is 'by construction' the X-ray beam focus point and then the Raman spot is brought confocal to it using its own (X', Y', Z') manipulator. The sample is then translated along its plane by piezo (X'', Y'') actuators in order to put the beams on the silicon substrate, mounted just aside the YAG. X'' is parallel to X and therefore normal to the plane defined by the two beams, while Y'' is perpendicular to it within the sample plane. The difference in the thicknesses of the two substrates, which has been measured previously, is taken into account by a correct translation of the sample along the X-ray beam (Y) and along the vertical axis (Z). Fine tuning of the laser focusing on the silicon substrate can then be carried out. Owing to the small convergence angles (horizontal and vertical) of the KB system, the size of the X-ray spot is not affected much by a small change in the longitudinal position of the sample along the X-ray beam. Typically, a variation of this position by 100 µm will result in a size variation of the spot of 0.3 µm. However, a slight variation of the sample height has a very large effect on the focusing of the laser beam because of its stronger convergence. This laser focusing is obtained finally by a small vertical adjustment of the Raman head, which does not change the position of the laser beam on the sample much. Now, by moving only the piezo (X'', Y'') actuator, we can describe any point on the surface sample using the two techniques, without losing the focusing of the beams.

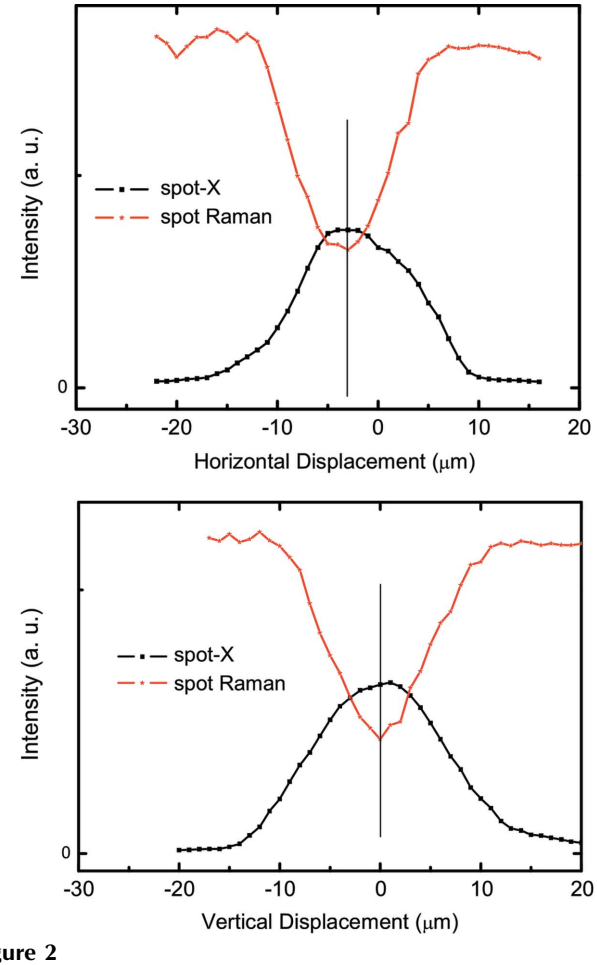

Figure 2
Scans along two perpendicular directions on the sample plane of a 16 µm titanium dot measured at the same time by XRF ($K\alpha$ Ti fluorescence) and by Raman spectroscopy (521 cm^{-1} silicon signal).

Scanning the sample along one direction and recording the intensities of the titanium fluorescence signal and of the 521 cm^{-1} silicon Raman line at each sample step (every micrometer) determines how the two beams are confocal. This appears as a direct feasibility test of a coupled µ-X-ray and µ-Raman experiment. Fig. 2 shows the two measured intensities as a function of the displacement of the piezo actuator when crossing a 16 µm Ti dot along a horizontal line (X'') and perpendicular to it within the sample plane (Y'', 'vertical' in the figure). The overall shape of the curves is the result of the convolution of the size of the Ti dot and the sizes of the beams. After alignment, as expected the maximum of the Ti $K\alpha$ X-ray fluorescence peak coincides within less than 1 µm with the minimum of the silicon Raman signal which is screened by the metal dot. The width of the two curves is consistent with a spot footprint of around 7 µm for the two beams, taking into account, for the 'vertical' component, the 45° incidence angle. The differences between the four curves indicates some asymmetry of the beams, and probably a slightly wider laser beam than X-ray beam.

4. Application to the study of rock minerals

Coupling two structural and local techniques, with microanalysis capabilities, is of major importance in the study of very poorly defined materials like soils or rocks: very different types of mineral species can coexist on a scale of a few micrometers. As an example of application, we show here results obtained from a thin slide of a gneiss rock collected in the upper part of the Joeri valley (Silvretta mountain area, Switzerland). The elements of interest are aluminium and silicon, which are the major elements of the minerals forming gneiss (quartz, feldspar and mica). Therefore we have equipped the monochromator with a pair of KTP(110) crystals and set the focusing of the beamline to almost the same values as for the titanium tests. From XRF cartography of a given area of the sample showing the distribution of Si, Al and Na elements, several points of interest (POIs) have been chosen. They are characterized by different Si/Al and Na ratios as shown in Fig. 3, which gathers all the XRF spectra collected at 1900 eV. POI1 is the only one which exhibits Si, Al and Na with a Si/Al ratio close to 4, as measured from Fig. 3. POI2 and POI3 have a much lower Si/Al ratio, around 2, while POI4 exhibits significantly less aluminium and no sodium.

X-ray absorption near-edge structure (XANES) spectra at the silicon K-edge have then been registered at these POIs,

together with the Raman spectra, and the results are gathered in Figs. 4, 5 and 6, where relevant reference spectra are also shown. All the XANES spectra are corrected for the dead-time of the fluorescence detector, and from self-absorption effects assuming the chemical formula of the identified phase, using the procedure developed by Haskel (1999).

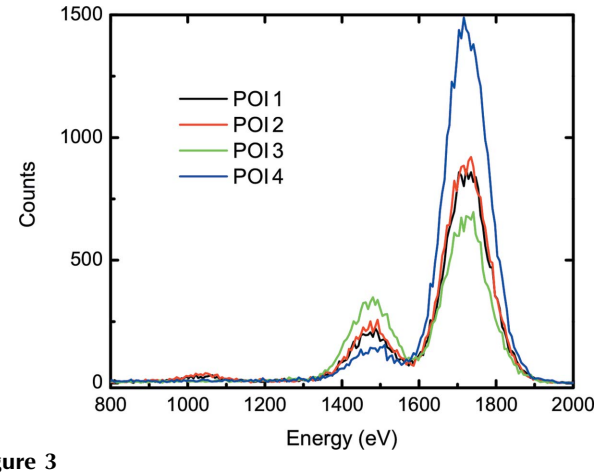

Figure 3
XRF spectra for different points of interest. Excitation has been made at 1900 eV.

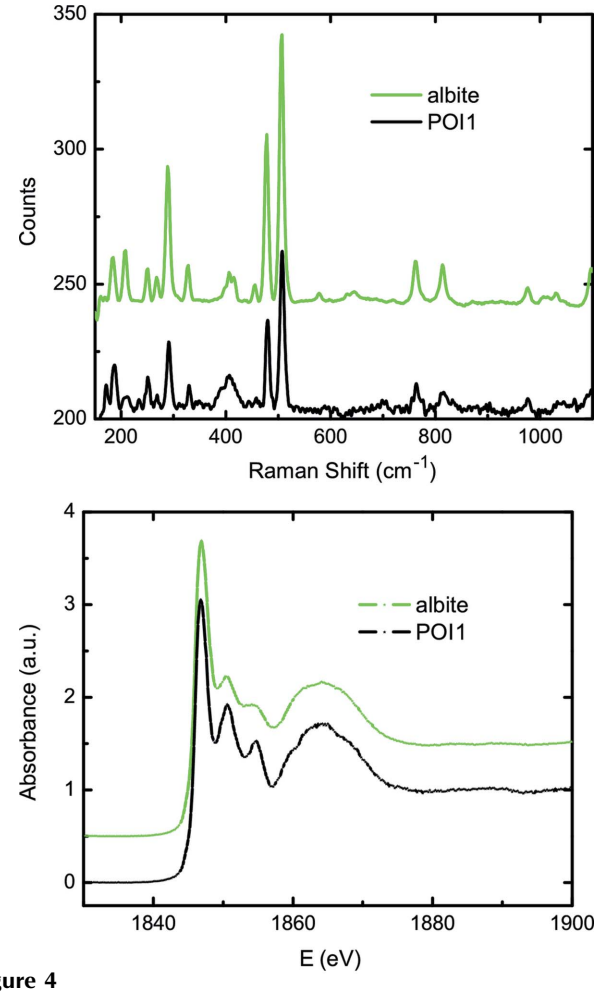

Figure 4
The Raman (top) and XAS (bottom) at the silicon *K*-edge of POI1, together with the spectra of albite.

POI1 definitely shows (Fig. 4) the XAS signatures of albite ($NaAlSi_3O_8$) but, on the scale of the spot size (here typically 7 μm), this albite is not pure or well crystallized since the XANES is slightly different from that of the model compound. The corresponding μ-Raman spectrum shows the lines attributed to albite, but as for XAS the spectrum is not that of pure albite. No further analysis has been carried out here, since the important conclusion is the consistency of the two results.

Fig. 5 shows the results obtained from POI2 and POI3, which have similar Si/Al ratios although much lower than those on the preceding locations. From the general shapes of the XANES spectra, and without any complementary information on the sample related to its geochemical origin, their attribution seems very ambiguous. The overall signal is definitely that of a phyllosilicate (Castro *et al.*, 1997): in that structure the common lamellar arrangement of tetrahedrons of silica and octahedrons of alumina gives rise to spectral fingerprints that are clearly different from those observed for other aluminosilicate compounds, as for instance the albite shown in Fig. 4. On the other hand, the μ-Raman spectra of these two locations, shown in Fig. 5 (top), are without any

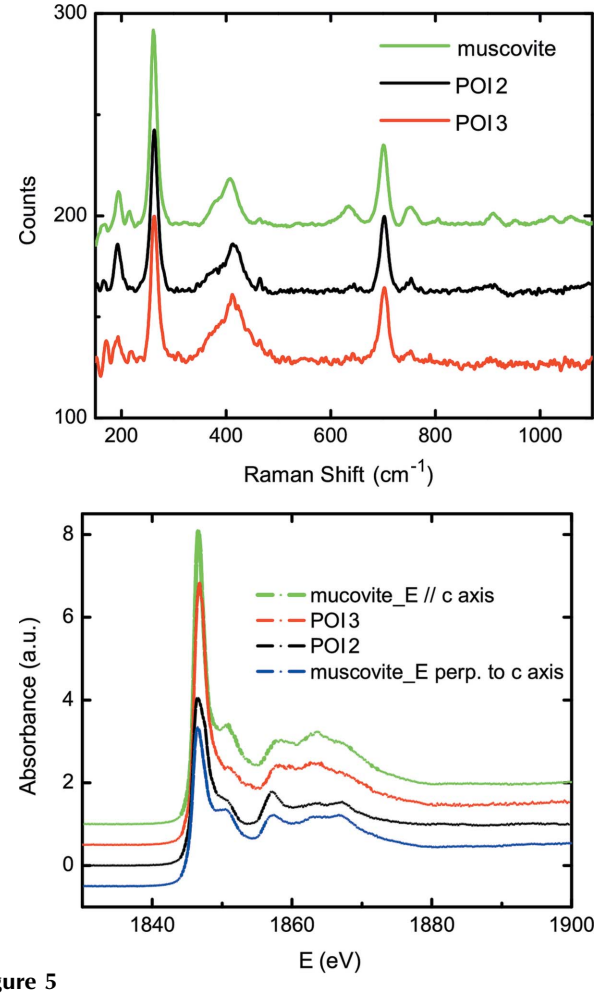

Figure 5
The Raman (top) and XAS (bottom) at the silicon *K*-edge of POI2 and POI3, together with the spectra of muscovite. XAS spectra for the two POIs are similar with the two polarized spectra of the reference.

ambiguity identical and present the characteristic fingerprints of muscovite, ruling out the presence of other phyllosilicates, in particular kaolinite. To overcome this apparent discrepancy between XANES and Raman results, and taking into account the lamellar nature of phyllosilicates, we have then recorded the XANES of the muscovite reference with the photon electric field in the plane of the sheets and normal to them. These spectra are shown in Fig. 5. It appears that the two POIs correspond to two orientations of the layers in the rock. Therefore we have here a situation where the Raman result has helped to lift an ambiguity that XANES could not resolve alone. The next example illustrates in more detail the consequences of this important parameter of X-ray absorption experiments, which could blur some experimental results: the polarization effect.

Fig. 6(*a*) shows the elemental mappings for aluminium and silicon around the location of POI4. POI4 is located at the border of an isolated region around 30 µm wide. XRF shows mostly Si with a small contribution from Al. The Raman spectrum (Fig. 6*b*, left) is characteristic of that of quartz crystal, despite the presence of aluminium which is probably involved in a compound much less Raman-active. The silicon XANES (Fig. 6*b*, right) presents some similarity with that of quartz powder, but rather seems to be almost identical to that of pure quartz with its *c*-axis oriented along the photon electric field. In order to confirm this interpretation, we have registered the same spectrum on the same spot after setting the Apple-II undulator polarization to vertical. This ability of the insertion device allows us to change the polarization on the sample without moving it. The two spectra are fully in line with the two experimental polarized data obtained with a macro beam on an oriented single crystal of quartz and modelled by full multiple-scattering calculations (Taillefumier *et al.*, 2002). As was the case for the XANES results on the spots of Fig. 5 compared with a muscovite model compound, we have, with the micro beam, strong polarization effects since all these minerals are often micro-crystallized. In several cases the reactivity of a solid strongly depends upon the crystallographic plane exposed to the reactants and this behavior can be of a fundamental importance in the studies of pollution processes of soils. Polarized µ-XAS experiments, which now can be easily and rapidly recorded on the micrometer scale by

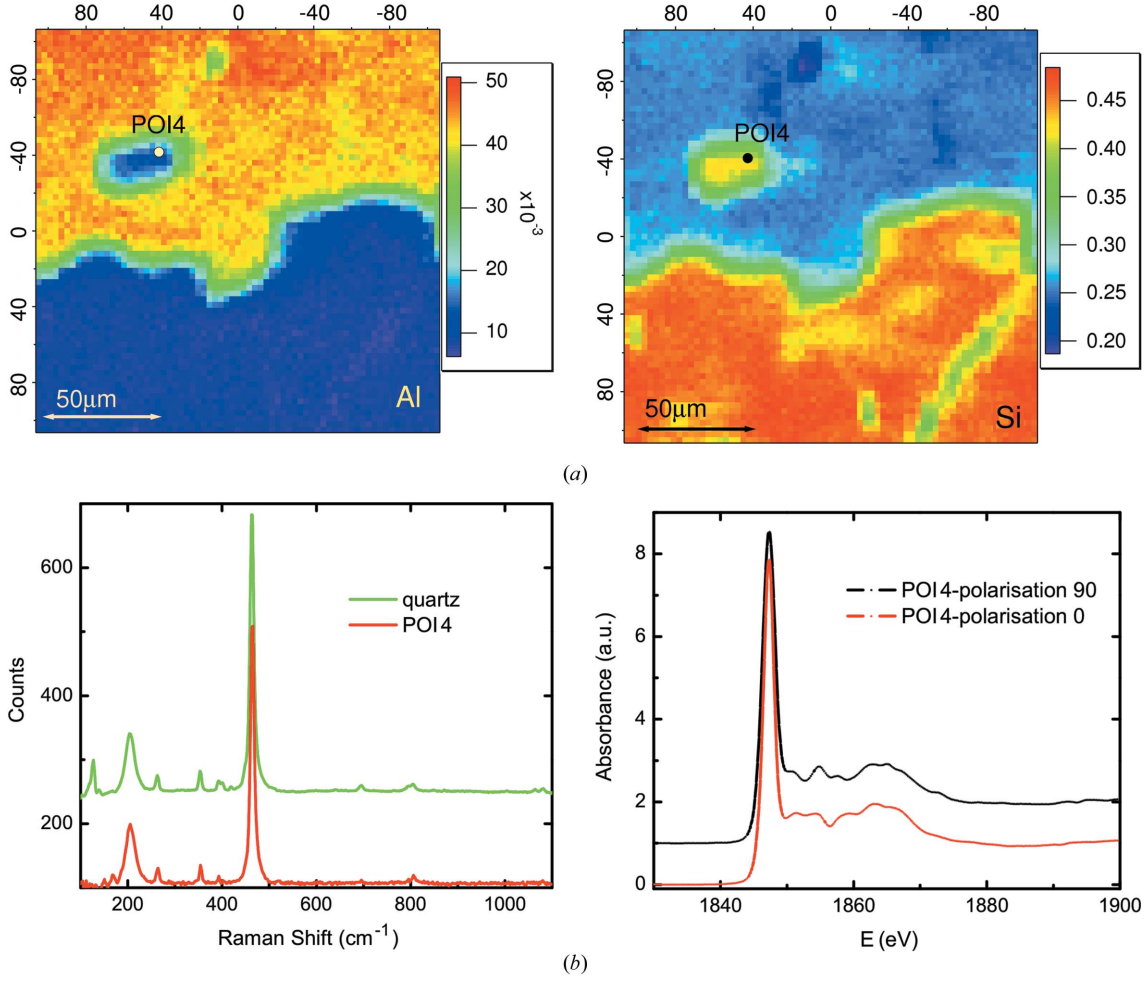

Figure 6
(*a*) XRF maps of Al and Si collected at 1900 eV in the area of POI4 which appears as a silicon-only compound. The map size is 210 µm × 210 µm, collected in steps of 3 µm × 3 µm and 1 s dwell time. (*b*) The Raman spectra (left) identify POI4 as pure quartz only. Si *K*-edge XANES (right) collected in POI4 in 0° and 90° polarization are identical to those already published (Taillefumier *et al.*, 2002).

tuning the insertion device, give a set of complementary information. The micro-sample which is studied can then be described beyond its crystallographic nature, as illustrated by the preceding example.

Therefore these experiments clearly show that, by recording XAS and Raman spectra on the same experimental set-up at an identical position, we reinforce conclusions which could only be extracted from one kind of experiment.

5. Perspectives and conclusions

The main limitations of the present experiments are the following.

(i) As these experiments were considered as first tests, we used the actual experimental chamber with the constraint of setting the laser beam orthogonal to the X-ray beam. Any change of this geometry would have required large modifications of the flange which forms the interface between the KB system and the experimental chamber. However, by decreasing the angle between the two beams, we would obtain a much better use of the focusing properties of the two optics since the incidences could then be made almost normal for the two beams. This is part of the improvements we are planning to make on the whole experimental set-up.

(ii) As mentioned previously, the focusing characteristics of the two beams are very different, and therefore great attention has to be paid to the variations of the height of the sample surface relative to the plane defined by the piezo actuators. When the sample is not perfectly flat, automated corrections taking into account the actual flatness of the sample have to be implemented.

(iii) At the low X-ray energies delivered by the LUCIA beamline, between 1 and 8 keV, the sample depth probed by XAS amounts typically to a few micrometers when the detection is made through the fluorescence, or a few hundreds of angstroms in the case of a total electron yield collection. For a confocal Raman apparatus, most of the signal originates from a depth of about 2 μm when a 50:1 objective lens like ours is used. However, all these figures may depend upon the optical absorption of the sample and the concentration of the element of interest. We then have here an intrinsic cause of uncertainty in comparing the two results. However, in both cases the situation is much better than in the comparison between transmission XRD (usually performed at higher X-ray energies) and Raman spectroscopy: in that case the sampling depths could be very different.

Despite the limitations of the present experimental set-up, we have proved here that combining two structural complementary techniques like Raman spectroscopy and XAS on the scale of a few micrometers could largely improve the interpretation of the results of each technique. Micro-cartography is a preliminary step that gives a first idea on the species present in the sample and enlightens the regions of interest before using the two structural techniques together. While, if one is only interested in a static point of view, one could argue that the same sample location could be analyzed separately, the situation definitely appears different when one wants to follow carefully the evolution of a very peculiar region of the sample under an external constraint, and particularly when this constraint is difficult to apply in a reproducible manner. That type of study makes full use of the simultaneous recording of the two signals.

This work was performed at the Swiss Light Source, Paul Scherrer Institut, Villigen, Switzerland. We are grateful to the machine and beamline groups whose outstanding efforts have made these experiments possible. We acknowledge also Dr A. Hofmann (University Lille) for providing the thin-section rock sample.

References

Briois, V., Belin, S., Villain, F., Bouamrane, F., Lucas, H., Lescouëzec, R., Julve, M., Verdaguer, M., Tokumoto, M. S., Santilli, C. V., Pulcinelli, S. H., Carrier, X., Krafft, J. M., Jubin, C. & Che, M. (2005). *Phys. Scr.* T**115**, 38–44.

Briois, V., Lützenkirchen-Hecht, D., Villain, F., Fonda, E., Belin, S., Grisebock, B. & Frahm, R. (2005). *J. Phys. Chem. A*, **109**, 320–329.

Castro, M. A., Alba, M. D., Alvero, R., Becerro, A. I., Munoz-Paez, A. & Trillo, J. M. (1997). *J. Phys. IV*, **7**(C2), 827–828.

Davies, R. J., Burghammer, M. & Riekel, C. (2005). *Appl. Phys. Lett.* **87**, 264105.

Flank, A.-M., Cauchon, G., Lagarde, P., Bac, S., Janousch, M., Wetter, R., Dubuisson, J.-M., Idir, M., Langlois, F., Moreno, T. & Vantelon, D. (2006). *Nucl. Instrum. Methods Phys. Res. B*, **246**, 269–274.

Haskel, D. (1999). *FLUO*, http://www.aps.anl.gov/xfd/people/haskel/fluo.html.

Schroer, C. G., Kuhlmann, M., Günzler, T. F., Lengeler, B., Richwin, M., Griesebock, B., Lützenkirchen-Hecht, D., Frahm, R., Ziegler, E., Mashayekhi, A., Haeffner, D., Grunwaldt, J.-D., Baiker A. & Schröder, W. (2005). *Phys. Scr.* T**115**, 1026–1028.

Taillefumier, M., Cabaret, D., Flank, A.-M. & Mauri, F. (2002). *Phys. Rev. B*, **66**, 195107.

Thompson, A. C., Underwood, J. H., Anderson, E. H., McHugo, S. A. & Lai, B. (2001). *Proc. SPIE*, **4145**, 16–21.